HHS Public Access

Author manuscript

J Surfactants Deterg. Author manuscript; available in PMC 2024 May 01.

Published in final edited form as:

J Surfactants Deterg. 2023 May ; 26(3): 387–399. doi:10.1002/jsde.12654.

Assessment of antimicrobial activity of melittin encapsulated in bicontinuous microemulsions prepared using renewable oils

Madison A. Oehler[1], **Douglas G. Hayes**[1], **Doris H. D'Souza**[2], **Manjula Senanayake**[3], **Viswanathan Gurumoorthy**[3], **Sai Venkatesh Pingali**[3], **Hugh M. O'Neill**[3], **Wim Bras**[3], **Volker S. Urban**[3]

[1]Department of Biosystems Engineering and Soil Science, University of Tennessee, Knoxville, Tennessee, USA

[2]Department of Food Science, University of Tennessee, Knoxville, Tennessee, USA

[3]Neutron Scattering Division, Oak Ridge National Laboratory, Oak Ridge, Tennessee, USA

Abstract

The objective of this study is to demonstrate that melittin, a well-studied antimicrobial peptide (AMP), can be solubilized in an active form in bicontinuous microemulsions (BMEs) that employ biocompatible oils. The systems investigated consisted of Winsor-III and -IV BME phases composed of Water/Aerosol-OT (AOT)/Polysorbate 85/isopropyl myristate and a Winsor-IV BME employing Polysorbate 80 and limonene. We found that melittin resided in an α-helix-rich configuration and was in an apolar environment for the AOT/Polysorbate 85 Winsor-III system, suggesting that melittin interacted with the surfactant monolayer and was in an active conformation. An apolar environment was also detected for melittin in the two Winsor-IV systems, but to a lesser extent than the Winsor-III system. Small-angle X-ray scattering analysis indicated that melittin at a concentration of 1.0 g/L_{aq} in the aqueous subphase of the Winsor-IV systems led to the greatest impact on the BME structure (e.g., decrease of quasi-periodic repeat distance and correlation length and induction of interfacial fluidity). The antimicrobial activity of the Polysorbate 80 Winsor-IV system was evaluated against several bacteria prominent in chronic wounds and surgical site infections (SSIs). Melittin-free BMEs inhibited the growth of all tested

Correspondence: Douglas G. Hayes, Department of Biosystems Engineering and Soil Science, University of Tennessee, 2506 E.J. Chapman Drive, Knoxville, TN 37996, USA. dhayes1@utk.edu.

AUTHOR CONTRIBUTIONS

The concept and funding for this paper came from Doris H. D'Souza, Douglas G. Hayes, and Volker S. Urban. The design of the experiments was performed by Doris H. D'Souza, Douglas G. Hayes and Madison A. Oehler. Madison A. Oehler, Viswanathan Gurumoorthy and Hugh M. O'Neill collected and analyzed CD and fluorescence data. Madison A. Oehler, Manjula Senanayake, Sai Venkatesh Pingali, Wim Bras, and Douglas G. Hayes performed the data collection and analysis of SAXS data. Douglas G. Hayes and Madison A. Oehler co-wrote the first draft of the manuscript. All authors participated in the revision of the manuscript.

CONFLICT OF INTEREST

The authors declare no conflict of interest.

ETHICS STATEMENT

No human or animal subjects were used in this research.

SUPPORTING INFORMATION

Additional supporting information can be found online in the Supporting Information section at the end of this article.

bacteria due to its oil, limonene, while the inclusion of 1.0 g/L_{aq} of melittin in the BMEs enhanced the activity against several bacteria. A further increase of melittin concentration in the BMEs had no further enhancement. These results demonstrate the potential utility of BMEs as a delivery platform for AMPs and other hydrophilic and lipophilic drugs to inhibit antibiotic-resistant microorganisms in chronic wounds and SSIs.

Graphical Abstract

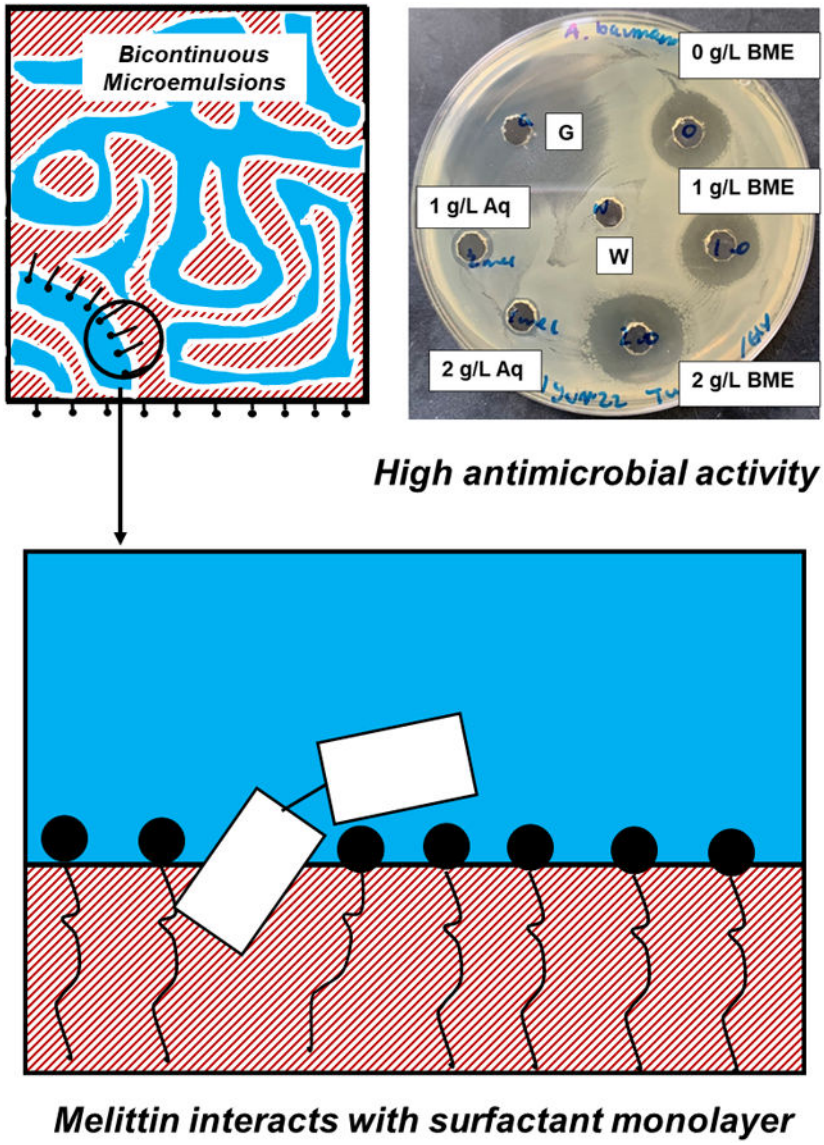

Keywords

antimicrobial activity; antimicrobial peptides; bicontinuous microemulsions; melittin; small-angle X-ray scattering

INTRODUCTION

Chronic wounds, defined as wounds that do not heal in an appropriate amount of time, and surgical site infections (SSI) result in many extended hospitalizations and fatalities each year and lead to discomfort and lowered quality of life for patients (Frykberg & Banks, 2015). Methods to prevent these infections such as cleaning and preparing medical tools have had minimal success in preventing infections (Fife & Carter, 2012; Zimlichman et al., 2013). SSIs have been described as one of the most common healthcare associated infections with most being preventable (Bagnall et al., 2009; Leaper, 2010). Chronic wounds and SSIs are caused by gram-positive and gram-negative bacteria that originate from the patient or external environment (Gupta et al., 2021). Further, antibiotic treatments applied to SSIs and chronic wounds have become less successful because of the rise in antibiotic-resistant bacteria, such as methicillin-resistant *Staphylococcus aureus* (MRSA; Gupta et al., 2021). New measures are required to reduce the negative impacts.

Antimicrobial peptides (AMP) are a possible solution to combat the rise in antibiotic-resistant microorganisms in the treatment of chronic wounds and SSIs. AMPs are naturally occurring amphipathic oligopeptides, many of which are positively-charged, that are found in humans, animals, or synthetically created and possess biological activity against bacteria, viruses, fungi, and tumors (Kang et al., 2019; Ramazi et al., 2022). AMPs operate by disrupting the packing arrangements of biomembranes in prokaryotic invaders through their insertion into negatively charged phospholipid bilayers. Although AMPs have many beneficial functions, such as wound healing, they have not been adopted universally because of their potential toxicity to humans, sensitivity to environmental factors, folding problems, ineffective encapsulation and delivery, and high costs (Bahar & Ren, 2013; Thapa et al., 2020). AMPs currently approved by the U.S. Food and Drug Administration (FDA) include gramicidin (a component found in several ophthalmic formulations), daptomycin, colistin, nisin, melittin, and polymxyins (Huan et al., 2020). Many others have been researched but were not successful in passing each round of clinical trials (Dijksteel et al., 2021).

Selection and design of delivery systems for AMPs requires further study. Delivery systems may include polymeric materials, surfactant and lipid dispersion/self-assembly systems, peptide self-assembly systems, and other formulations (Nordström & Malmsten, 2017). Delivery systems that have been proposed specifically to treat wounds include nanoparticles, hydrogels, creams, and ointments (Huan et al., 2020). Many systems approved for the delivery of AMPs are applied through intradermal, subcutaneous, or transdermal injections (Anil & Kannan, 2018). These methods can be invasive and, in some cases, cause pain to the patients. Additional and newer systems are required to encapsulate and effectively topically deliver AMPs in a biologically active form.

A possible topical delivery treatment system for AMPs are bicontinuous microemulsions (BMEs). Microemulsions are dynamic, optically clear and thermodynamically stable nanoscale dispersions of oil-in-water or water-in-oil formed by surfactant monolayers (Sjöblom et al., 1996). BMEs consist of elongated nanodomains of oil and water formed by surfactants equally balanced in hydrophilicity and lipophilicity. The balance can be readily achieved through proper selection (i.e., optimization) of tuning parameters, such

as temperature for alkyl ethoxylate surfactants and salinity for ionic surfactants, with three-phase ME systems formed at low surfactant concentration (Winsor-III, or W_{III} systems, composed of BME middle phases in equilibrium with water and oil excess phases) and 1-phase BMEs (W_{IV} systems) formed at higher surfactant concentrations (Nguyen & Sabatini, 2011). The laboratories of Jeffrey Harwell and David Sabatini have been instrumental in developing strategies for optimization of BMEs (Attaphong & Sabatini, 2017; Chen et al., 2022; Do et al., 2015; Nguyen & Sabatini, 2009; Phan et al., 2010). It is therefore a pleasure to participate in this Special Issue of *Journal of Surfactants and Detergents* to honor both. BMEs have been employed for many applications, including enhanced oil recovery (Marquez et al., 2019), nanomaterials (Shiba et al., 2022), blending of immiscible polymers (Kulshreshtha et al., 2022), protein purification (Hayes et al., 2017), and chemical and biochemical reactions (Bose et al., 2022; Wang & Huang, 2021). BMEs are particularly well-suited for drug delivery due to their ability to solubilize large amounts of polar and apolar drugs simultaneously (Choi et al., 2021; Peng et al., 2021).

We have previously been successful in encapsulating melittin, a well-studied model positively-charged AMP consisting of 26 amino acids that is rich in α-helix secondary structure when bound to biomembranes (Guha et al., 2021; Habermann & Jentsch, 1967; Moreno & Giralt, 2015; Teixeira et al., 2012), into BMEs at concentrations exceeding 5 g/L through the construction of W_{III} systems formed by anionic surfactants (Hayes et al., 2018). The molecular structure of melittin is given in Figure S1 (Hong et al., 2019). We found that BME-encapsulated melittin resides in a highly folded, α-helical, form, indicating it is likely interacting with the surfactant monolayers, enabling it to be biologically active. However, above a threshold concentration (~1–2 g/L), melittin appeared to be less intimately associated with the surfactant monolayers, leading to a reduction of folding (Sharma et al., 2017; Sharma et al., 2019).

The goal of this research is to demonstrate that melittin can be solubilized in an active form within W_{III} or W_{IV}-based BME systems where the alkane oils employed previously are replaced by isopropyl myristate (IPM) or limonene and to test the resultant BMEs for their antimicrobial activity against gram-positive and gram-negative bacteria commonly found in SSIs and chronic wounds. Analysis of BMEs and related delivery systems (e.g., cubosomes) for antimicrobial activity has been rarely studied (de Assis et al., 2020). Two systems were created using an anionic surfactant Aerosol-OT (AOT; Liu et al., 2009; Yanyu et al., 2012). Another system was created using a nonionic surfactant, Polysorbate 80 (de Campo et al., 2004). Both systems were successful in encapsulating aqueous melittin up to and over 2.0 g/L.

MATERIALS AND METHODS

Materials

AOT (sodium bis(2-ethylhexyl) sulfosuccinate, ≥97% pure), Polysorbate (Tween®) 80 (polyoxyethylene (20) sorbitan monooleate), Polysorbate (Tween®) 85 (polyoxyethylene (20) sorbitan trioleate), (*R*)-(+)-limonene (97% pure), isopropyl myristate (IPM) (≥98% pure), glycerol (≥99% pure), and melittin from bee venom (≥85% HPLC), a + 6-charged peptide (pI = 12.01, MW = 2846 g/mol), were purchased from Sigma-Aldrich (Milwaukee,

WI, USA). Because melittin is a slightly toxic and slightly irritating (acute oral and dermal ecotoxicity, Category 3), nitrile gloves were employed when handling. Ethanol, Falcon™ 96-well non-treated U-shaped bottom polypropylene plates, tryptic soy broth (TSB), tryptic soy agar (TSA), phosphate buffered saline (PBS), Mueller Hinton agar (MHA), blank paper disks, ciprofloxacin disks, and gentamicin antibiotic liquid were purchased from Fisher Scientific (Pittsburgh, PA, USA). Frozen bacteria cultures of *Escherichia coli* K-12 (American Type Culture Collection [ATCC]—11229), *Staphylococcus aureus* (ATCC—51740), *Enterococcus faecium* (ATCC—19434), and *Pseudomonas aeruginosa* (ATCC—27853) were from the University of Tennessee (UT) Food Science Department. The culture of *Acinetobacter baumannii* (ATCC—19606) was purchased from Microbiologics (St. Cloud, MN, USA) and provided to us by Dr. Sree Rajeev of the UT Center for Veterinary Medicine. *Streptococcus pyogenes* was a gift from Washington University, St. Louis, USA. All bacterial strains were aseptically transferred in TSB and incubated for 24 h at 37°C thrice. Bacteria were also streaked for isolation on TSA and isolated colonies were transferred to TSB. Mark-tubes made of Quartz glass, 0.1 mm wall thickness were purchased from Charlessupper (Westborough, MA, USA). Deionized water was used throughout.

Preparation of BMEs

Three BME systems, two of which were W_{IV} and the other being W_{III}, were prepared at room temperature 22 ± 1°C (measured daily). The compositions and conditions, listed in Table 1, are based on conditions provided in the literature (de Campo et al., 2004; Liu et al., 2009; Yanyu et al., 2012), with salinity scans employed to optimize the AOT/Polysorbate 85 W_{III} system. Moreover, optimal conditions produce the most rapid equilibration of the W_{III} system, leading to reduced denaturation of melittin. The systems contained either IPM or limonene as oil; two of the systems contained an anionic/nonionic surfactant blend (AOT/Polysorbate 85) and the other contained only Polysorbate 80 as surfactant. These systems were formed by mixing the correct amount of surfactant into the oil phase. When the surfactants were fully dissolved, an aqueous solution with or without melittin was added and mixed until equilibrated (W_{IV} systems within 1 min; W_{III} system within 15 min). For the W_{III} system, 1.0 or 2.0 g/L_{aq} aqueous solution was one of the ingredients mixed together to form the three-phase system. Composition of the W_{III} BME phases is given in Table 2. For the W_{IV} BMEs, melittin was added in the form of 1.0 or 2.0 g/L_{aq} aqueous solutions, with the resultant melittin concentrations for the overall BMEs (g/L_{BME}) given in Table 3. Aqueous controls employed in the spectroscopic and antimicrobial assay measurements consisted of 1.0 and 2.0 g/L_{aq} melittin in aqueous solution containing the same salinity and pH of the corresponding BME system's aqueous subphase, with glycerol included in the aqueous controls for the Polysorbate 80 W_{IV} system.

Melittin concentration measurement

Melittin concentration for the bottom phase of AOT/Polysorbate 85 W_{III} systems formed by aqueous solution (per Table 1) containing melittin at specified concentrations was determined by a spectrophotometric assay employed previously (Gomez del Rio & Hayes, 2011). A 50 μl aliquot was removed from the bottom phase of the W_{III} system and added to a microcentrifuge tube followed by 1000 μl of acetone to remove the surfactants. After

the mixture was centrifuged, acetone was discarded, and the residual solid was placed in an incubator at 30°C until fully dried. The solid was rehydrated with 50 μl of 85 mM NaCl solution. Samples were then added to Coomassie Blue reagent in a 1.0 cm pathlength cuvette. Spectrophotometric measurements were conducted on a UV-1700 instrument from Shimadzu (Kyoto, Japan). Measurements were taken at 595 nm and compared to a calibration curve prepared from aqueous solutions of bovine serum albumin (BSA) standards of known concentrations from Fisher. The concentration of melittin in the middle, BME phase was calculated using volume fractions of the W_{III} system, measured using a ruler for the system after its placement in tall (4 cm) quartz cuvettes of pathlength 1 mm after 72 h of equilibration (two replicates). It was assumed that melittin did not partition to the top phase. Mass balance was used to determine the percentage of melittin achieved in the middle, BME phase.

Circular dichroism spectroscopy

CD measurements were taken at 22°C using a model J-810 spectropolarimeter from JASCO (Halifax, NS, Canada) to determine the secondary structure of melittin. Measurements were taken for the AOT/Polysorbate 85 W_{III} system for melittin concentrations of 0.5, 1.0, and 2.0 g/L_{aq}. Similar to a previous study, a 0.1 mm pathlength cell was used to measure the wavelength of the system from 180 to 250 nm at 100 nm/min, with a bandwidth of 1 nm, data pitch of 0.5 nm, and 10 accumulations (Hayes et al., 2018). For each BME sample, 40 μl was extracted from the middle phase of the system and added to the 0.1 mm pathlength cell. Data collected for BMEs without melittin was subtracted from the data for BMEs with melittin. Two replicates of each sample were averaged and plotted for comparison.

Fluorescence spectroscopy

Fluorescence emission spectra were taken for BMEs and corresponding aqueous phases at 22°C using a SpectraMax i3 microplate reader from Molecular Devices (San Jose, CA, USA). A clear polypropylene 96 well plate was used to measure multiple samples, with a 100 μl aliquot of sample loaded into each well. Samples were excited at 285 nm and the absorbance was measured across a wavelength of 310–450 nm at 2 nm intervals. Each sample was analyzed in triplicate and spectra were averaged. Spectra for melittin encapsulated in BMEs were corrected by subtracting the spectra for BMEs without melittin.

Small-angle X-ray scattering

Small-angle X-ray scattering (SAXS) was used to analyze the structure of BMEs in the presence and absence of melittin for the systems listed in Table 1. SAXS measurements were carried out at 23°C on a Xeuss 3.0 instrument from Xenocs (Santa Barbara, CA, USA) equipped with D2+ MetalJet X-ray source (Ga Ka, 9.2 keV, wavelength [λ] = 1.341 Å). The instrument measured across a Q range of 0.01 to 0.7 $Å^{-1}$. A volume of 100 μl of a BME sample was added to a 1.5 mm quartz capillary tube and sealed with epoxy resin. The tubes were placed vertically in the sample holder and aligned perpendicularly to the directions of the x-ray beam in transmission mode. SAXS data was analyzed by fitting the Teubner-Strey (T-S) model, commonly used for BMEs, to the main scattering peak (Schubert et al., 1994; Schubert & Strey, 1991). The model determines the quasi-periodic repeat distance (d), correlation length (ξ), amphiphilicity factor (f_a), and the bare bending modulus (κ_{theor}). The

parameter f_a represents the degree of ordering of the surfactant monolayers. Values below ~−0.5 represent high ordering, as would be seen in BMEs, while values approaching −1 are highly ordered, similar to lamellae. Similarly, values of κ_{theor} below ~k_BT, where k_B is Boltzmann's constant and T is temperature (absolute scale), represent fluid interfacial dynamics for surfactant monolayers, while higher values reflect more rigid interfaces. Further information on the T-S model and related parameters are provided in the Supporting Information. Data analysis was conducted using the software written by staff scientists at the National Institute of Standards and Technology (NIST), that uses Igor Pro (v.5.0.4.7, WaveMetrics, Lake Oswego, OR) as a platform (Kline, 2006).

Well diffusion assays

Each experiment was conducted at 22 ± 1°C and when incubation was used, the temperature was 37°C. Well diffusion assays (Zhang et al., 2009) were conducted under a flame to ensure no contamination to the samples. Pipette tips, forceps, and water (control) were sterilized in an autoclave (121°C) before use. TSA, TSB, PBS, and MHA were all prepared according to the manufacturer's guidelines. TSA and MHA were prepared weekly in 100 mm petri dishes. After autoclaving the TSA and MHA, they were allowed to cool for 15–20 min and a volume of 15 ml was added to each petri dish to ensure uniformity for the well diffusion assays. Frozen bacterial cultures were aseptically transferred to TSB and incubated for 24 h at 37°C thrice. The TSB cultures were streaked for isolation on TSA and isolated colonies were transferred to TSB for use in the antimicrobial assays. Before each well diffusion experiment bacteria cultures were aseptically transferred to fresh TSB 24 h in advance and incubated at 37°C.

Well diffusion experiments began by washing bacteria cultures. This occurred by transferring 1 ml of each TSB bacteria culture to a sterile microcentrifuge tube. Cultures were centrifuged for 1 min at 8000 rpm (5 cm radius) until a pellet was formed. The TSB was discarded in a waste bag and 2 ml of PBS was added to the bacterial pellet and vortexed until completely mixed. MHA plates were prepared by spread plating 0.1 ml of the washed bacterial culture, creating a lawn of bacteria over the agar. Wells were bored from the MHA using the back of a micropipette tip (5 mm diameter) and removed using sterilized forceps. Forceps were dipped in ethanol and flamed between each bacterium. There were seven wells created on each plate to allow for three treatments and four controls. The treatments were BME without melittin, BME with 1.0 and 2.0 g/L_{aq} melittin. The controls were water, gentamicin (5.0 g/L), and 1.0 and 2.0 g/L melittin in aqueous solution. A volume of 60 μl was taken from each treatment or control and added to its respectively marked well. Plates were allowed to sit for 15 min before placed in an incubator for 24 h. After 24 h, plates were removed from the incubator, inverted, and zones of inhibition were measured. Zones of inhibition were measured by taking two perpendicular diameter measurements to the nearest mm and recorded for each well.

Statistical analysis

For SAXS data, errors for $I(Q)$ were calculated through the instrument software. Errors for all data are reported as the average ± standard deviation (95% confidence interval). Statistical analysis comparison tests for the antimicrobial activity assays via the Student T

test were completed using JMP, Version 16, SAS Institute Inc., Cary, NC. Statistical analyses were carried out on the comparison of the Polysorbate 80 W_{IV} system with and without melittin to determine if there was a significant difference in the treatments.

RESULTS AND DISCUSSION

Melittin incorporation into BMEs

Multiple BME systems containing biocompatible oils identified from the scientific literature were pre-screened for the incorporation of melittin. The most effective and robust systems observed from the pre-screening are listed in Table 1 and will be further discussed below. Visually, melittin was accepted into the W_{IV} systems without any precipitation or phase change. For the AOT/Polysorbate 85 W_{III} system, the salinity employed in our initial experiments was 100 mM NaCl. With the addition of melittin, the system transformed into a W_I system because the melittin made the surfactants more hydrophilic. A series of trials with salinity ranging from 60 to 100 mM NaCl were carried out. At 85 mM NaCl, a W_{III} system was achieved with all three concentrations of melittin tested. Additionally, for the AOT/Polysorbate 85 W_{III} system, lower concentrations of the surfactant were tested. But it was determined that 5% total surfactant concentration was optimal to create a W_{III} system. These results completed the objective of successfully encapsulating an AMP into the BMEs.

The partitioning of melittin to the middle, BME phase of the AOT/Polysorbate 85 W_{III} system was determined. Almost 100% of the melittin partitioned to the BME phase for each concentration of melittin tested (Table 2). Further, as the concentration of melittin was increased, the volume fraction of the BME phase decreased (Table 2 and Figure S2). An increase of melittin concentration increased the relative proportions of water in the BMEs (Table 2); moreover, as the melittin concentration increased, the volume fraction of the top, oil excess phase increased linearly to a much greater extent than the increase of the bottom, aqueous excess phase volume fraction (Figure S2). The decrease of BME phase volume fraction and strong partitioning of melittin into the W_{III} BME phase was also observed for other W_{III} systems based on alkane oils; but, in contrast to the current study, the BME phase became more apolar with the addition of melittin (Hayes et al., 2018). Because of the strong partitioning of melittin to the BME phase and decrease in volume of the BME phase, the melittin concentration in the BME phase was within 65%–85% of the initial aqueous phase melittin concentration despite the addition of oil (IPM) to water at a 1.2/1.0 vol/vol ratio (Table 2).

Conformation and microenvironment of melittin in BMEs

CD data were collected for melittin dissolved in the AOT/Polysorbate 85 W_{III} system and aqueous solutions comparable in concentration and salinity to the BME aqueous subphase. CD measurements were also attempted for the W_{IV} systems; however, the signal-to-noise ratio for the CD spectra was poor, presumably because of the high absorbance due to the higher surfactant concentrations for the W_{IV} systems. CD spectra for melittin at all three concentrations in BMEs possessed two minima occurring at 208 and 225 nm, consistent with high α-helical content (Figure 1; Wei et al., 2014). Melittin in an aqueous solution also had a minimum at 208 nm but not at 225 nm, with its spectra more closely resembling

β-sheet secondary structure (Greenfield, 2007). In aqueous solution, melittin exists as monomers or tetramers and has low α-helical content (Terwilliger & Eisenberg, 1982). This suggests that melittin was in its most active state when encapsulated in BMEs compared to the aqueous solution, a result that also observed for melittin residing in BMEs formed by alkane-based oils (Hayes et al., 2018), and in water-in-oil microemulsions (w/o-MEs; Oehman et al., 1996; Raghuraman & Chattopadhyay, 2003). This supported the hypothesis that BMEs serve as a biomembrane mimetic system because melittin was in its most active structure, α-helix, when encapsulated in the BME.

Fluorescence emission spectra of melittin in BMEs were collected for all systems listed in Table 1 and compared to aqueous solutions of melittin with similar composition and melittin concentration. Blue shifts were seen for melittin in the fluorescence emission spectra of each of BME system investigated relative to spectra of melittin in corresponding aqueous media, signifying that the location of melittin transitions to a more apolar environment when encapsulated in a BME compared to an aqueous solution. The blue shift was greater for the AOT/Polysorbate 85 W_{III} system (12 nm for 1.0 and 2.0 g/L_{aq} melittin; Figure 2) than for the W_{IV} systems (~4 nm). The results suggest that the melittin was residing within the surfactant monolayers of the BME systems, likely driven to this position by electrostatic attractive interactions between the positively charged amino acid residues of melittin and the sulfonate head group of AOT and hydrophobic interactions between melittin's apolar residues and the surfactant monolayers. Although Polysorbate 80 is uncharged, previous studies have shown that ethoxylated surfactants can possess a slightly negative charge in MEs (Vasudevan & Wiencek, 1996). Similarly, we found previously that the anionic surfactants AOT (in a mixed surfactant system with a cyclic ketal alkyl ethoxylate) and SDS induced blue shifts for melittin encapsulated in the W_{III} BME phase of 31 and 5 nm, respectively (Hayes et al., 2018). And in w/o-MEs, the maximum absorbance was slightly lower than achieved for the AOT/Polysorbate 85 W_{III} BME (346 nm): 330–340 nm (Raghuraman & Chattopadhyay, 2003). These results showed that melittin was interacting with the surfactant. In addition, the fluorescence intensity of melittin was slightly quenched for the W_{III} BME system. Quenching has also been observed in BMEs and w/o-microemulsions. The greater degree of quenching for the W_{IV} systems is likely attributable to the higher surfactant concentrations, leading to a smaller nanodomain size for the W_{IV} systems compared to the W_{III} BME (described in the next section). Similarly, the extent of quenching for melittin increased as the size of w/o-MEs decreased (Raghuraman & Chattopadhyay, 2003).

Effect of melittin incorporation on the structure of BMEs

The T-S model fit SAXS curves for all three BME phases reasonably well, demonstrating that BMEs likely formed rather than oil-in-water (o/w-) or w/o-microemulsions, which exist as spherical nanodroplets (Figure 3). Yet, an additional scattering feature occurred at high-Q for all samples, near 0.10–0.12 $Å^{-1}$. This feature is most evident in Figure 3 for the Polysorbate 80 W_{IV} system, due to the position of its main scattering curve being in a higher Q range compared to the other two. The secondary scattering at high-Q is more visible when the data is replotted in log–log coordinates (Figure S3). This feature does not appear to be attributable to multiple coherent scattering (Hayes et al., 2015; Silas & Kaler, 2003)

since the secondary scattering peak does not coincide with $2Q_{max}$, where Q_{max} refers to the Q position for the peak of the main scattering curve (Figures S3 and S4). The underlying cause of the high-Q feature was not determined. When fitting the SAXS data, a Q range was selected for fitting that did not have any contribution from the high-Q scattering peak. The fits for the two AOT/Polysorbate 85 systems were good, since the main scattering peaks are in the low-Q region. For the Polysorbate 80 W_{IV} system, although the fitting of the scattering curve was not as robust, the fit was sufficient to enable further analysis.

Values for parameters derived from the T-S models applied to the data of Figure 3 are given in Table 3. For the AOT/Polysorbate 85 systems, values of d and ξ were 400–700 Å and 100–300 Å, respectively. The values are ~2-fold lower than values previously measured for the water/AOT/ cyclic ketal alkyl ethoxylate/heptane system used for encapsulation of melittin, likely due to the decreased efficiency of surfactant resulting from poorer solvation of surfactant tails by IPM in the current study compared to heptane in the previous study (Hayes et al., 2018). Moreover, a ~2-fold higher overall surfactant concentration (5%) was needed to form robust W_{III} systems herein compared to the previous study (2% surfactant). As the melittin concentration is increased, both d and ξ decrease, reflecting decreased efficiency for the surfactant. This trend is likely due to ion pairing between melittin and AOT, a result that we have observed for melittin and other proteins in other W_{III} systems (Hayes et al., 2015, 2017, 2018, 2021). Values for f_a for the AOT/Polysorbate 85 W_{III} system were ≤ -0.59, suggesting ordered BMEs (Table 3). As the melittin concentration is increased, f_a increases and κ_{theor} decreases, similar in trend to what was observed for the AOT/CK-2,13 W_{III} system for the same melittin range and indicative of increased interfacial fluidity for the surfactant monolayers of the BMEs (Hayes et al., 2018).

For the AOT/Polysorbate W_{IV} system, values of d, ξ, f_a and κ_{theor} are significantly lower than corresponding values for the W_{III} system, trends attributable to the higher surfactant concentration of the W_{IV} system (Table 1; Schubert et al., 1994; Schubert & Strey, 1991). Although melittin has a smaller impact on the structure of BMEs for the W_{IV} systems compared to the W_{III} BMEs, significant changes were observed for both W_{IV} systems. For an increase of melittin concentration from 0.0 to 1.0 g/L_{aq}, trends follow those described above for the AOT/Polysorbate 85 W_{III} system (Table 3). However, a further increase of melittin concentration from 1.0 to 2.0 g/L_{aq} led to opposing trends. For the BME phase of the water/SDS/pentanol/dodecane W_{III} system, we also observed a similar reversal of trends when the melittin concentration was increased for the short- and long-range dynamics of BMEs, as measured using quasi-elastic neutron scattering and neutron spin-echo, respectively (Sharma et al., 2017, 2019). The changes were attributed to a more direct interaction of melittin with surfactant head groups and the surfactant monolayer at lower melittin concentrations, while at higher concentrations, a saturation of the interface occurred and additional melittin resided in aqueous solution near the surfactant interface, where they induced Debye shielding (Sharma et al., 2017, 2019).

For the Polysorbate 80 W_{IV} system, a similar trend occurs as is described above for the AOT/CK-2,13 W_{IV} system, with 1.0 g/L_{aq} serving as the melittin concentration for which trends reverse as one further increases the melittin concentration (Table 3). When observing the SAXS data (Figure 3), the scattering curve for 1.0 g/L_{aq} melittin is much flatter than

for the other concentrations. The Polysorbate 80 system was slightly less efficient than the AOT/Polysorbate 85 W_{IV} system, as observed by the slightly lower values of d and ξ, and its surfactant monolayers are slightly more ordered and rigid, as observed by the slightly lower f_a values and higher κ_{theor} values. In summary, melittin impacts the structure of BMEs through their direct interaction with surfactant head groups at the monolayer surface and a saturation of melittin at the interface occurs near 1.0 g/L_{aq}.

Analysis of the antimicrobial activity of melittin encapsulated in BMEs

Well diffusion was employed to evaluate inhibition of bacteria commonly encountered in chronic wounds and SSIs for the melittin loaded BMEs. The K12 strain of *E. coli* is found in the digestive tract of humans. Other assay methods investigated included disk diffusion, dilution and plating, and kinetic bacterial measurements. We found that MHA served as the best media option for the diffusion assays based on preliminary experiments. For well diffusion with the AOT/Polysorbate 85 systems, microbial inhibition was not observed, resulting from the adsorption of AOT to the walls of the well, which prohibited the diffusion of melittin and BMEs in the radial direction outward into the media. As a result, the antimicrobial activity of the AOT/Polysorbate 85 systems could not be assessed accurately.

The Polysorbate 80 W_{IV} system was successful in diffusing radially outward into the media with lawns of bacteria (Figure 4 and Table 4). This system produced zones of bacterial inhibition in the presence and absence of melittin, but with the inhibition zones being statistically significantly larger for the latter for most of the bacteria examined ($p < 0.05$). This finding supports the idea that melittin increased the effectiveness of the BMEs' ability to inhibit bacterial growth, perhaps as a penetration enhancer. Similarly, the encapsulation of the AMP LL-37 in a bicontinuous cubic phase (cubosomes) enhanced the AMP's antimicrobial activity (Gontsarik et al., 2016). The effectiveness of melittin-free, or unfilled, BMEs as an inhibitor may be attributable to the presence of limonene, which possesses significant antimicrobial activity (Espina et al., 2013). Similarly, the incorporation of essential oils such as limonene into w/o- or o/w-MEs has been reported to enhance antimicrobial activity compared to controls (Arellano et al., 2021; Han et al., 2021; He et al., 2022; Karadağ et al., 2022; Guo et al., 2020). Therefore, limonene and melittin are synergistic in their biological activity. In contrast, aqueous solutions of 1.0 or 2.0 g/L_{aq} melittin were not effective for inhibition of the tested bacteria (Table 4). BMEs were effective as inhibitors but not as effective as gentamicin, the positive control, a commonly used antibiotic known to be effective but can also produce side-effects to humans (Chaves & Tadi, 2022).

Statistical analysis showed significant differences between treatments between the BME with and without melittin for *E. coli* K12, *P. aeruginosa*, and *S. aureus* ($p < 0.05$; Table 4). When a 95% confidence interval was used, *A. baumanii*, *E. faecium*, and *S. pyogenes* showed no significant differences in their zones of inhibition when treated with the BME with and without melittin. However, there were significant differences when a 90% confidence interval was applied for *S. pyogenes* ($p = 0.07$). Ideally, researchers favor using a 95% confidence interval, though occasionally a 90% confidence interval can be used for smaller experimental sets. The statistical analysis was conducted on three replications

of the treatment on the bacteria. More replications could be done to further conclude the significance of the difference in zones of inhibition among the treatments. The differences between the 1.0 and 2.0 g/L_{aq} BME treatments were not statistically different. Therefore, 1.0 g/L_{aq} may be the optimal concentration of melittin to be effective in inhibiting bacterial growth when encapsulated in this BME system. The same concentration was observed via SAXS to minimize the T-S parameters ξ and d (Table 3), suggesting the structure of melittin and BMEs near 1 g/L_{aq} is optimal. Perhaps the successful performance of the Polysorbate 80 W_{IV} BME system may be related to rapid release kinetics due to the weak electrostatic attractive binding of melittin to the surfactant interface compared to the AOT/Polysorbate 85 systems (per fluorescence analysis, Figure 2). No selectivity was exhibited for the melittin-loaded BMEs toward either gram-positive or gram-negative microorganisms.

CONCLUSIONS

Melittin, a commonly studied AMP, was successfully encapsulated in BMEs possessing biocompatible oils: Water/AOT/Polysorbate 80/IPM through both W_{III} and W_{IV} systems and Water/Polysorbate80/ethanol/glycerol/limonene (W_{IV}). In these systems, melittin resided in a more apolar environment than aqueous media, suggesting its localization near the surfactant monolayers, and for the W_{III} system, CD analysis demonstrated that melittin was in an active, α-helical-rich, conformation. SAXS analysis also reflected intimate interactions between melittin and BMEs' surfactant monolayers, leading to increased interfacial fluidity and lower surfactant efficiency. The Polysorbate 80 W_{IV} system was evaluated for antimicrobial activity against several bacteria that are prominent in chronic wounds. The BMEs alone possessed significant antimicrobial activity against all bacteria tested due to its limonene component. The addition of melittin led to a further enhancement of antimicrobial activity against several gram-positive and gram-negative bacteria. An optimal melittin concentration of ~1 g/L_{aq} was observed for maximizing the impact on BME structure and antimicrobial activity.

This research showed promise in using biocompatible BMEs as a drug delivery platform for topical delivery to chronic wounds and SSIs, to deliver AMP and polar and apolar drugs. Our results demonstrated the synergy between essential oils and AMPs, with the latter perhaps serving the role of a penetration enhancing agent. Further testing and development of additional systems is warranted.

Although there was some difficulty encountered when testing BMEs with antimicrobial assays, progress was made. A major challenge was that the surfactant AOT strongly adsorbed to surfaces within the testing system, which hindered diffusion in and out of the BMEs. Additional consideration is needed on the selection of polymeric materials or container used for the assays to prevent or at least reduce adsorption.

Supplementary Material

Refer to Web version on PubMed Central for supplementary material.

ACKNOWLEDGMENTS

The authors acknowledge funding from the National Institutes of Health (Grant 5R03AI154314-02). Dr. Durgesh Kumar Rai (Xenocs, Inc., Holyoke, MA) assisted with the SAXS data collection. The authors acknowledge resources supported by the Center for Structural Molecular Biology funded by DOE Biological and Environmental Research (project ERKP291). This research used resources at the High Flux Isotope Reactor and Spallation Neutron Source, a DOE Office of Science User Facility operated by the Oak Ridge National Laboratory.

Funding information

National Institute of Allergy and Infectious Diseases, Grant/Award Number: 5R03AI154314-02; Oak Ridge National Laboratory, Grant/Award Number: Center for Struct. Mol. Biol (ERKP291)

DATA AVAILABILITY STATEMENT

Data employed for preparing the figures for this manuscript are available at https://doi.org/10.5061/dryad.1g1jwsv1d.

REFERENCES

Anil L, Kannan K. Microemulsion as drug delivery system for peptides and proteins. J Pharm Sci Res. 2018;10:16–25.

Arellano S, Law B, Friedman M, Ravishankar S. Essential oil microemulsions inactivate antibiotic-resistant *salmonella* Newport and spoilage bacterium *lactobacillus casei* on iceberg lettuce during 28-day storage at 4°C. Food Control. 2021;130:108209. 10.1016/j.foodcont.2021.108209

Attaphong C, Sabatini DA. Optimized microemulsion systems for detergency of vegetable oils at low surfactant concentration and Bath temperature. J Surfactant Deterg. 2017;20:805–13. 10.1007/s11743-017-1962-8

Bagnall NM, Vig S, & Trivedi P (2009). Surgical-Site Infect Surg (Oxford), 27:426–430, doi:10.1016/j.mpsur.2009.08.007.

Bahar AA, Ren D. Antimicrobial peptides. Pharmaceuticals. 2013;6: 1543–75. 10.3390/ph6121543 [PubMed: 24287494]

Bose AL, Bhattacharjee D, Goswami D. Mixed micelles and bicontinuous microemulsions: promising media for enzymatic reactions. Colloids Surf B Biointerfaces. 2022;209:112193. 10.1016/j.colsurfb.2021.112193 [PubMed: 34768101]

Chaves BJ, Tadi P. Gentamicin. Treasure Island, FL: StatPearls Publishing; 2022 [Accessed October 10, 2022]. Available from: https://www.ncbi.nlm.nih.gov/books/NBK557550

Chen C, Shen H, Harwell JH, Shiau B-J. Characterizing oil mixture and surfactant mixture via hydrophilic-lipophilic deviation (HLD) principle: an insight in consumer products development. Colloids Surf A Physicochem Eng Asp. 2022;634:127599. 10.1016/j.colsurfa.2021.127599

Choi K-O, Choi SJ, Lee S. Characterization of phase and diffusion behaviors of oil, surfactant, and co-surfactant ternary systems for lipid-based delivery carriers. Food Chem. 2021;359:129875. 10.1016/j.foodchem.2021.129875 [PubMed: 33940469]

de Assis KMA, da Silva Leite JM, de Melo DF, Borges JC, Santana LMB, dos Reis MML, et al. Bicontinuous microemulsions containing Melaleuca alternifolia essential oil as a therapeutic agent for cutaneous wound healing. Drug Deliv Transl Res. 2020;10:1748–63. 10.1007/s13346-020-00850-0 [PubMed: 32924099]

de Campo L, Yaghmur A, Garti N, Leser ME, Folmer B, Glatter O. Five-component food-grade microemulsions: structural characterization by SANS. J Colloid Interface Sci. 2004;274:251–67. 10.1016/j.jcis.2004.02.027 [PubMed: 15120300]

Dijksteel GS, Ulrich MMW, Middelkoop E, Boekema BKHL. Review: lessons learned from clinical trials using antimicrobial peptides (AMPs). Front Microbiol. 2021;12:616979–9. 10.3389/fmicb.2021.616979 [PubMed: 33692766]

Do LD, Attaphong C, Scamehorn JF, Sabatini DA. Detergency of vegetable oils and semi-solid fats using microemulsion mixtures of anionic extended surfactants: the HLD concept and cold water applications. J Surfactant Deterg. 2015;18:373–82. 10.1007/s11743-014-1659-1

Espina L, Gelaw TK, de Lamo-Castellví S, Pagán R, García-Gonzalo D. Mechanism of bacterial inactivation by (+)-limonene and its potential use in food preservation combined processes. PLOS ONE. 2013;8:e56769. 10.1371/journal.pone.0056769 [PubMed: 23424676]

Fife CE, Carter MJ. Wound care outcomes and associated cost among patients treated in US outpatient wound centers: data from the US wound registry. Wounds. 2012;24:10–7. [PubMed: 25875947]

Frykberg RG, Banks J. Challenges in the treatment of chronic wounds. Adv Wound Care (New Rochelle). 2015;4:560–82. 10.1089/wound.2015.0635 [PubMed: 26339534]

Gomez del Rio JA, Hayes DG. Protein extraction by Winsor-III microemulsion systems. Biotechnol Prog. 2011;27:1091–100. 10.1002/btpr.611 [PubMed: 21695808]

Gontsarik M, Buhmann MT, Yaghmur A, Ren Q, Maniura-Weber K, Salentinig S. Antimicrobial peptide-driven colloidal transformations in liquid-crystalline Nanocarriers. J Phys Chem Lett. 2016; 7:3482–6. 10.1021/acs.jpclett.6b01622 [PubMed: 27541048]

Greenfield NJ. Using circular dichroism spectra to estimate protein secondary structure. Nat Protoc. 2007;1:2876–90. 10.1038/nprot.2006.202

Guha S, Ferrie RP, Ghimire J, Ventura CR, Wu E, Sun L, et al. Applications and evolution of melittin, the quintessential membrane active peptide. Biochem Pharmacol. 2021;193:114769. 10.1016/j.bcp.2021.114769 [PubMed: 34543656]

Guo L, Fang Y-q, Liang X-r, Xu Y-y, Chen J, Li Y-h, et al. Influence of polysorbates (tweens) on structural and antimicrobial properties for microemulsions. Int J Pharm. 2020;590:119939. 10.1016/j.ijpharm.2020.119939 [PubMed: 33011247]

Gupta BB, Soman KC, Bhoir L, Gadahire M, Patel B, Ahdal J. The burden of methicillin resistant *Staphylococcus aureus* in surgical site infections: a review. J Clin Diagn Res. 2021;15:PE01–6. 10.7860/jcdr/2021/46922.14891

Habermann E, Jentsch J. Sequence analysis of melittin from tryptic and peptic degradation products. Hoppe Seylers Z Physiol Chem. 1967;348:37–50. [PubMed: 5592400]

Han Y, Chen W, Sun Z. Antimicrobial activity and mechanism of limonene against *Staphylococcus aureus*. J Food Saf. 2021;41: e12918. 10.1111/jfs.12918

Hayes DG, Anunciado DB, Ye R, Williams RND, O'Neill HM, Pingali SV, et al. Incorporation of membrane proteins into bicontinuous microemulsions through Winsor-III system-based extraction. J Surfactant Deterg. 2021;24:649–60. 10.1002/jsde.12500

Hayes DG, Gomez del Rio JA, Ye R, Urban VS, Pingali SV, O'Neill HM. Effect of protein incorporation on the nanostructure of the bicontinuous microemulsion phase of Winsor-III systems: a small-angle neutron scattering study. Langmuir. 2015;31: 1901–10. 10.1021/la504606x [PubMed: 25603188]

Hayes DG, Ye R, Dunlap RN, Anunciado DB, Pingali SV, O'Neill HM, et al. Bicontinuous microemulsions as a biomembrane mimetic system for melittin. Biochim Biophys Acta Biomembr. 2018; 1860:624–32. 10.1016/j.bbamem.2017.11.005 [PubMed: 29138064]

Hayes DG, Ye R, Dunlap RN, Cuneo MJ, Pingali SV, O'Neill HM, et al. Protein extraction into the Bicontinuous microemulsion phase of a water/SDS/Pentanol/Dodecane Winsor-III system: effect on nanostructure and protein conformation. Colloids Surf B Biointerfaces. 2017;160:144–53. 10.1016/j.colsurfb.2017.09.005 [PubMed: 28922633]

He X, Chen J, Li Y, Meng Y, Fang S, Fang Y. Preparation of water-in-oil (W/O) cinnamaldehyde microemulsion loaded with epsilon-polylysine and its antibacterial properties. Food Biosci. 2022;46: 101586. 10.1016/j.fbio.2022.101586

Hong J, Lu X, Deng Z, Xiao S, Yuan B, Yang K. How Melittin inserts into cell membrane: conformational changes, inter-peptide cooperation, and disturbance on the membrane. Molecules. 2019;24: 1775. 10.3390/molecules24091775 [PubMed: 31067828]

Huan Y, Kong Q, Mou H, Yi H. Antimicrobial peptides: classification, design, application and research Progress in multiple fields. Front Microbiol. 2020;11:582779. 10.3389/fmicb.2020.582779 [PubMed: 33178164]

Kang X, Dong F, Shi C, Liu S, Sun J, Chen J, et al. DRAMP 2.0, an updated data repository of antimicrobial peptides. Scientific Data. 2019;6:148. 10.1038/s41597-019-0154-y [PubMed: 31409791]

Karadağ AE, Üstündağ Okur N, Demirci B, Demirci F. Rosmarinus officinalis L. essential oil encapsulated in new microemulsion formulations for enhanced antimicrobial activity. J Surfactant Deterg. 2022;25:95–103. 10.1002/jsde.12549

Kline SR. Reduction and analysis of SANS and USANS data using IGOR Pro. J Appl Cryst. 2006;39:895–900. 10.1107/s0021889806035059

Kulshreshtha A, Hayward RC, Jayaraman A. Impact of composition and placement of hydrogen-bonding groups along polymer chains on blend phase behavior: coarse-grained molecular dynamics simulation study. Macromolecules. 2022;55:2675–90. 10.1021/acs.macromol.2c00055

Leaper DJ. Surgical-site infection. Br J Surg. 2010;97:1601–2. 10.1002/bjs.7275 [PubMed: 20878944]

Liu H, Wang Y, Lang Y, Yao H, Dong Y, Li S. Bicontinuous cyclosporin a loaded water-AOT/tween 85-isopropylmyristate microemulsion: structural characterization and dermal pharmacokinetics *in vivo*. J Pharm Sci. 2009;98:1167–76. 10.1002/jps.21485 [PubMed: 18729203]

Marquez R, Antón R, Vejar F, Salager J-L, Forgiarini AM. New interfacial rheology characteristics measured using a spinning drop Rheometer at the optimum formulation. Part 2. Surfactant–oil–water systems with a high volume of middle-phase microemulsion. J Surfactant Deterg. 2019;22:177–88. 10.1002/jsde.12245

Moreno M, Giralt E. Three valuable peptides from bee and wasp venoms for therapeutic and biotechnological use: melittin, apamin and mastoparan. Toxins. 2015;7:1126–50. 10.3390/toxins7041126 [PubMed: 25835385]

Nguyen TT, Sabatini DA. Formulating alcohol-free microemulsions using Rhamnolipid biosurfactant and Rhamnolipid mixtures. J Surfactant Deterg. 2009;12:109–15. 10.1007/s11743-008-1098-y

Nguyen TT, Sabatini DA. Characterization and emulsification properties of Rhamnolipid and Sophorolipid biosurfactants and their applications. Int J Mol Sci. 2011;12:1232–44. [PubMed: 21541055]

Nordström R, Malmsten M. Delivery systems for antimicrobial peptides. Adv Colloid Interface Sci. 2017;242:17–34. 10.1016/j.cis.2017.01.005 [PubMed: 28159168]

Oehman A, Davydov R, Backlund B-M, Langel U, Graeslund A. A study of melittin, motilin and galanin in reversed micellar environments, using circular dichroism spectroscopy. Biophys Chem. 1996;59:185–92. 10.1016/0301-4622(95)00122-0 [PubMed: 8867338]

Peng K, Sottmann T, Stubenrauch C. Gelled non-toxic bicontinuous microemulsions as promising transdermal drug carriers. Mol Phys. 2021;119:e1886363. 10.1080/00268976.2021.1886363

Phan TT, Harwell JH, Sabatini DA. Effects of triglyceride molecular structure on optimum formulation of surfactant-oil-water systems. J Surfactant Deterg. 2010;13:189–94. 10.1007/s11743-009-1155-1

Raghuraman H, Chattopadhyay A. Organization and dynamics of melittin in environments of graded hydration: a fluorescence approach. Langmuir. 2003;19:10332–41. 10.1021/la035126z

Ramazi S, Mohammadi N, Allahverdi A, Khalili E, Abdolmaleki P. A review on antimicrobial peptides databases and the computational tools. Database. 2022;2022:baac011. 10.1093/database/baac011 [PubMed: 35305010]

Schubert KV, Strey R. Small-angle neutron scattering from microemulsions near the disorder line in water/formamide–octane-C_iE_j systems. J Chem Phys. 1991;95:8532–45. 10.1063/1.461282

Schubert KV, Strey R, Kline SR, Kaler EW. Small angle neutron scattering near Lifshitz lines: transition from weakly structured mixtures to microemulsions. J Chem Phys. 1994;101:5343–55. 10.1063/1.467387

Sharma VK, Hayes DG, Gupta S, Urban VS, O'Neill HM, Pingali SV, et al. Incorporation of Melittin enhances interfacial fluidity of Bicontinuous microemulsions. J Phys Chem C. 2019;123: 11197–206. 10.1021/acs.jpcc.9b00103

Sharma VK, Hayes DG, Urban VS, O'Neill HM, Tyagi M, Mamontov E. Nanoscopic dynamics of bicontinous microemulsions: effect of membrane associated protein. Soft Matter. 2017; 13:4871–80. 10.1039/C7SM00875A [PubMed: 28631792]

Shiba S, Yoshimoto S, Hashiguchi S, Kunitake M, Kato D, Niwa O, et al. Porous gold nanomesh films electrodeposited in toluene-based dynamic soft template. Electrochim Acta. 2022;426: 140761. 10.1016/j.electacta.2022.140761

Silas JA, Kaler EW. Effect of multiple scattering on SANS spectra from bicontinuous microemulsions. J Colloid Interface Sci. 2003; 257:291–8. 10.1016/S0021-9797(02)00059-0 [PubMed: 16256483]

Sjöblom J, Lindberg R, Friberg SE. Microemulsions—Phase equilibria characterization, structures, applications and chemical reactions. Adv Colloid Interface Sci. 1996;65:125–287. 10.1016/0001-8686(96)00293-X

Teixeira V, Feio MJ, Bastos M. Role of lipids in the interaction of antimicrobial peptides with membranes. Prog Lipid Res. 2012;51: 149–77. 10.1016/j.plipres.2011.12.005 [PubMed: 22245454]

Terwilliger TC, Eisenberg D. The structure of melittin. I. Structure determination and partial refinement. J Biol Chem. 1982;257: 6010–5. [PubMed: 7076661]

Thapa RK, Diep DB, Tønnesen HH. Topical antimicrobial peptide formulations for wound healing: current developments and future prospects. Acta Biomater. 2020;103:52–67. 10.1016/j.actbio.2019.12.025 [PubMed: 31874224]

Vasudevan M, Wiencek JM. Mechanism of the extraction of proteins into tween 85 nonionic microemulsions. Industr Eng Chem Res. 1996;35:1085–9. 10.1021/ie950328e

Wang R, Huang X. Anionic-surfactant-stabilized hydrophobic ionic-liquid-based Bicontinuous microemulsion as a medium for enzymatic oxidative polymerization of aniline. ACS Omega. 2021;6: 20699–709. 10.1021/acsomega.1c03150 [PubMed: 34396015]

Wei Y, Thyparambil AA, Latour RA. Protein helical structure determination using CD spectroscopy for solutions with strong background absorbance from 190 to 230 nm. Biochim Biophys Acta. 2014;1844:2331–7. 10.1016/j.bbapap.2014.10.001 [PubMed: 25308773]

Yanyu X, Fang L, Qineng P, Hao C. The influence of the structure and the composition of water/AOT-Tween 85/IPM microemulsion system on transdermal delivery of 5-fluorouracil. Drug Dev Ind Pharm. 2012;38:1521–9. 10.3109/03639045.2012.654795 [PubMed: 22324326]

Zhang H, Shen Y, Weng P, Zhao G, Feng F, Zheng X. Antimicrobial activity of a food-grade fully dilutable microemulsion against *Escherichia coli* and *Staphylococcus aureus*. Int J Food Microbiol. 2009;135:211–5. 10.1016/j.ijfoodmicro.2009.08.015 [PubMed: 19717202]

Zimlichman E, Henderson D, Tamir O, Franz C, Song P, Yamin CK, et al. Health care–associated infections: a meta-analysis of costs and financial impact on the US health care system. JAMA Intern Med. 2013;173:2039–46. 10.1001/jamainternmed.2013.9763 [PubMed: 23999949]

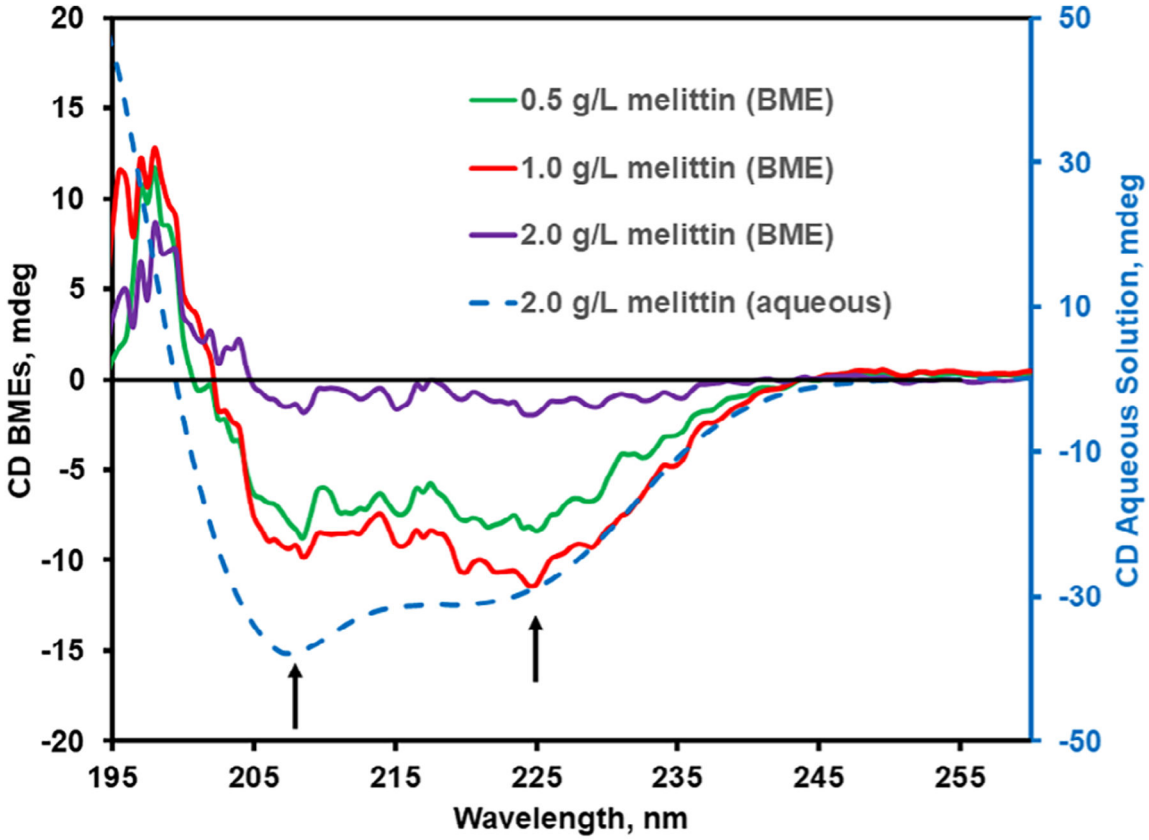

FIGURE 1.

Circular dichroism spectra of melittin solubilized in the bicontinuous microemulsions (BME) phase of the AOT/Polysorbate 85 Winsor-III system and in aqueous media corresponding to the BME aqueous subphase (22°C). Melittin concentrations for BMEs listed in the legend correspond to the aqueous solution employed to prepare BME; overall concentrations in the BMEs are listed in Table 2. Minima for α-helices, 208 and 225 nm, are indicated in the figures through arrows

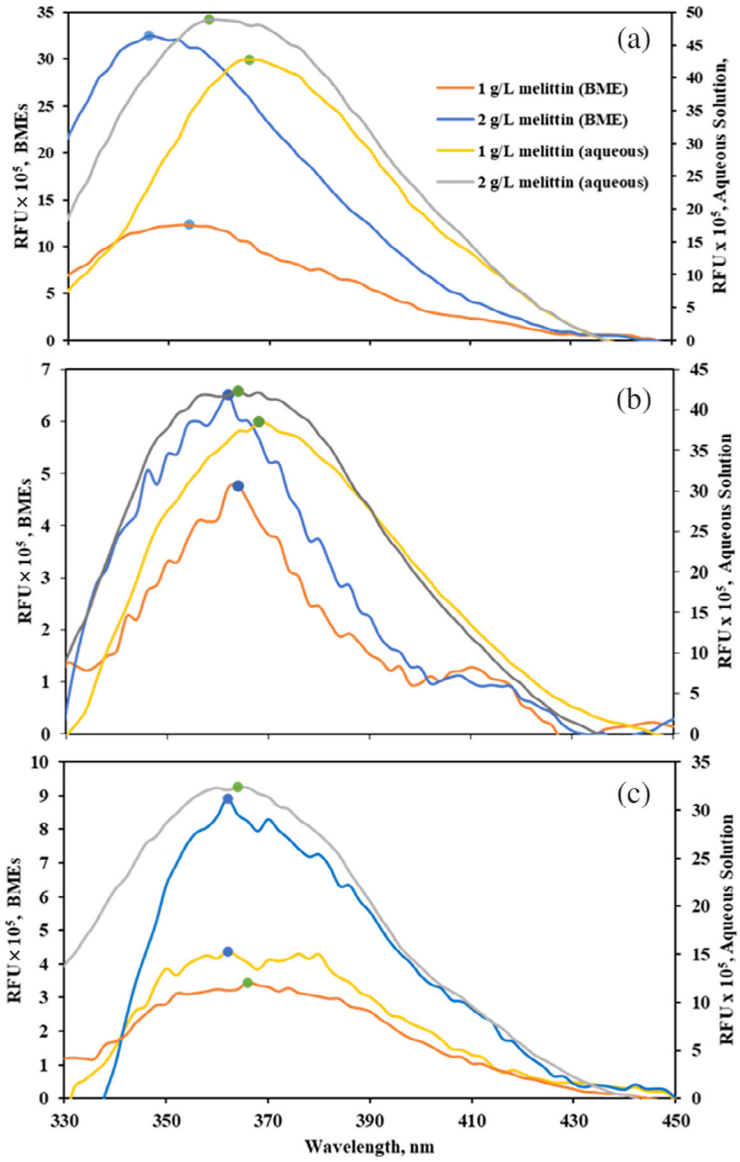

FIGURE 2.

Fluorescence emission spectra for melittin solubilized in bicontinuous microemulsions (BMEs) formed by the (a) AOT/Polysorbate 85 Winsor-III, (b) AOT/Polysorbate 85 Winsor-IV and (c) Polysorbate 80 Winsor-IV systems and in aqueous media corresponding to the BME aqueous subphase of BMEs (22°C). The excitation wavelength was 295 nm. Melittin concentrations for BMEs listed in the legend correspond to the aqueous solution employed to prepare BME; overall concentrations in the BMEs are listed in Tables 2 and 3 for figure (a) and figures (b) and (c), respectively. The aqueous solutions of Figure 3c include the presence of glycerol

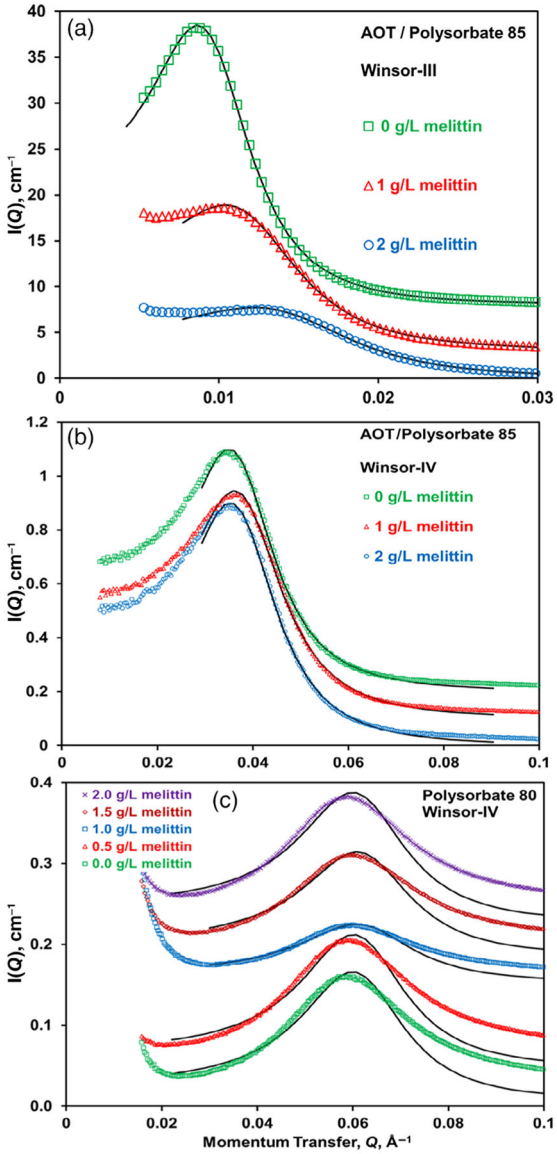

FIGURE 3.

SAXS data for bicontinuous microemulsions (BMEs) as a function of the melittin concentration in the aqueous phase at 22°C. Curves represent the fit of the Teubner-Strey model to the main scattering peak. A scaler (in cm^{-1}) was added to the scattering data to improve visualization: Figure (a): 7 and 3 for 0.0 and 1.0 g/L_{aq} melittin, respectively; Figure (b): 0.2 and 0.1 for 0.0 and 1.0 g/L_{aq}, respectively; Figure (c) 0.04, 0.15, 0.18 and 0.22 for 0.5, 1.0, 1.5, and 2.0 g/L_{aq}, respectively. Melittin concentrations for BMEs listed in the legend correspond to the aqueous solution employed to prepare BME; overall concentrations in the BMEs are listed in Tables 2 and 3 for Figure (a) and Figures (b) and (c), respectively

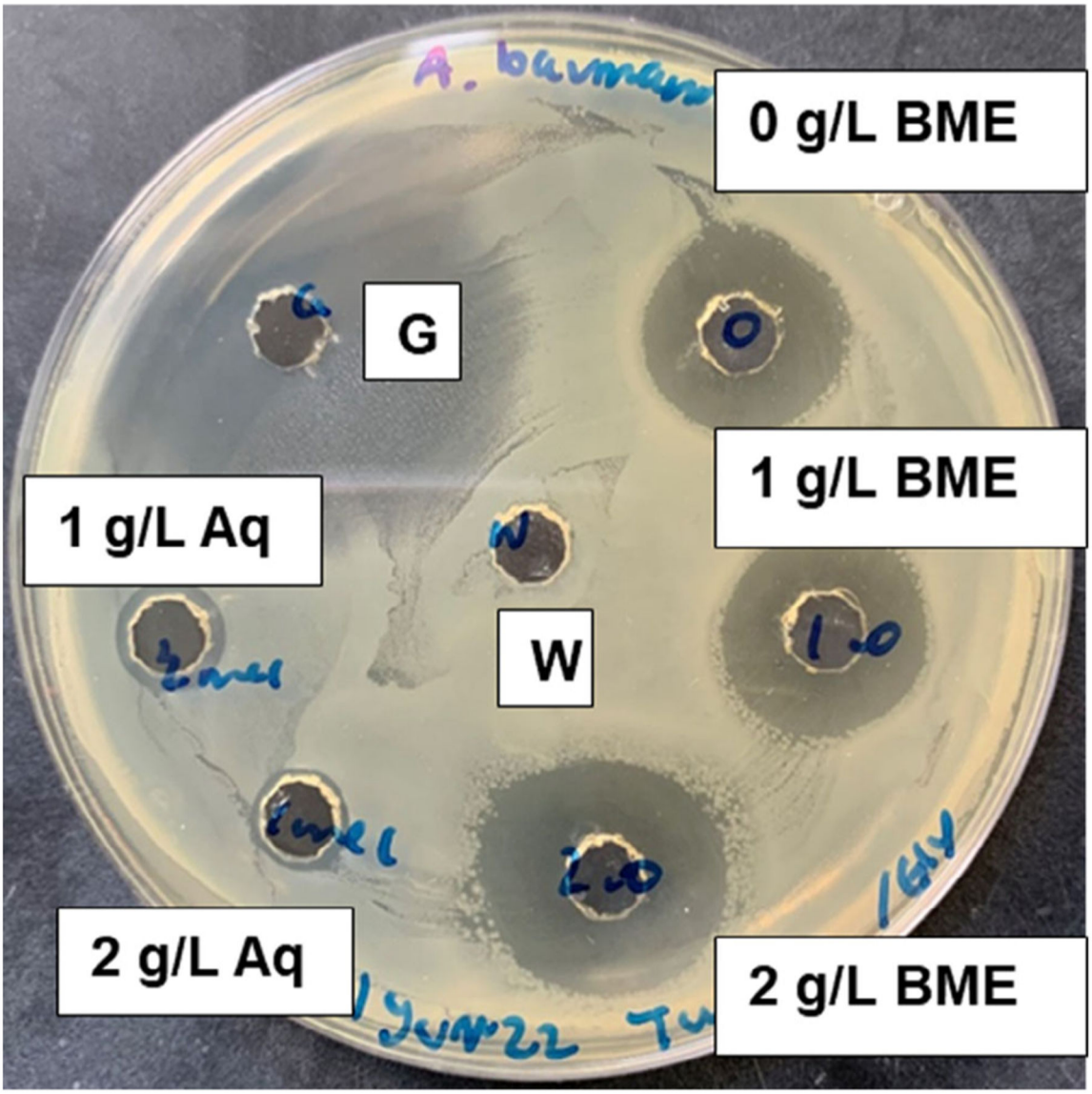

FIGURE 4.

Well diffusion assay against *Acinetobacter baumannii* using melittin encapsulated in Polysorbate Winsor-IV systems or corresponding aqueous solutions at 22°C, with the melittin concentration (referring to the volume of the bicontinuous microemulsions aqueous subphase) given in the labels. *G* and *W* refers to gentamicin (positive control) and water (negative control), respectively. Wells are 5 mm in diameter

TABLE 1

Microemulsions systems investigated for the encapsulation of melittin in bicontinuous microemulsions (BMEs)[a]

System name	Surfactant 1	Surfactant 2	Cosolvent	Oil	ω_W [b]	ω_{S1}	ω_{S2}	ω_{CS}	ω_O	References
AOT/Polysorbate 85 Winsor-III	Aerosol-OT	Polysorbate 85	None	IPM	47.5[c]	3.3	1.7		47.5	(Liu et al., 2009; Yanyu et al., 2012)
AOT/Polysorbate 85 Winsor-IV	Aerosol-OT	Polysorbate 85	None	IPM	30.0	13.3	6.7		50.0	(Liu et al., 2009; Yanyu et al., 2012)
Polysorbate 80 Winsor-IV	Polysorbate 80	None	Ethanol /glycerol 2.05 wt/wt	Limonene	39.6	21.4		31.9	7.1	(de Campo et al., 2004)

[a] Symbols: ω_X mass fraction of component *x* for entire system; subscripts: *W*, *S*1, *S*2, *CS*, and *O* refer to water, surfactant 1, surfactant 2, cosolvent, and oil, respectively.

[b] Aqueous phase consisted of 5 mM sodium phosphate buffer, pH 6.9.

[c] Aqueous phase also contained 85 mM NaCl.

TABLE 2

Melittin concentration and water volume fraction of the middle (bicontinuous microemulsions, BME) phase for the Water/AOT/Polysorbate 85/IPM Winsor-III system at 22°C[a]

Melittin concentration in initial aqueous phase, g/L_{aq}	Melittin extracted to BME phase %	Melittin concentration in BME phase, g/L	Volume % of BME phase	Volume % of water in BME phase[b,c]
0.0	-	-	72.5 ± 4.2	48.9 ± 4.9
1.0	99.8 ± 0.1	0.7 ± 0.0	66.8 ± 0.8	55.1 ± 1.6
2.0	99.6 ± 0.1	1.5 ± 0.0	57.4 ± 0.8	56.3 ± 1.6
3.0	99.6 ± 0.1	2.4 ± 0.0	53.9 ± 0.9	60.2 ± 1.6
4.0	99.7 ± 0.1	3.4 ± 0.3	51.2 ± 4.5	56.7 ± 8.2

[a]Each measurement was performed in triplicate, with errors being <10%.

[b]On a surfactant-free basis.

[c]The water volume % on a surfactant-free basis for the overall Winsor-III system is 46.0%.

TABLE 3

Parameter values derived from the Teubner-Strey model fit applied to SAXS data[a]

[Melittin]$_{aq}$, g/L$_{aq}$[b]	[Melittin]$_{BME}$, g/L$_{BME}$[c]	Correlation length, ξ (Å)	Quasi-periodic repeat distance, d (Å)	Amphiphilicity factor, f_a	Bending modulus, κ_{theor}/kT
AOT/Polysorbate 80, Winsor-III					
0.0	0.0	250.6 ± 0.2	659.6 ± 0.2	−0.701 ± 0.003	1.14 ± 0.0004
1.0	0.7	182.5 ± 0.2	535.1 ± 0.2	−0.642 ± 0.004	1.05 ± 0.001
2.0	1.5	140.2 ± 0.2	444.1 ± 0.2	−0.595 ± 0.006	0.986 ± 0.001
AOT/Polysorbate 80, Winsor-IV					
0.0	0.00	87.8 ± 0.2	170.6 ± 0.1	−0.825 ± 0.008	0.926 ± 0.001
1.0	0.28	82.8 ± 0.2	164.8 ± 0.1	−0.818 ± 0.007	0.908 ± 0.001
2.0	0.56	85.9 ± 0.2	169.0 ± 0.1	−0.821 ± 0.008	0.919 ± 0.001
Polysorbate 80, Winsor-IV					
0.0	0.00	75.8 ± 0.2	102.4 ± 0.04	−0.912 ± 0.008	0.996 ± 0.001
0.5	0.25	75.2 ± 0.2	102.1 ± 0.04	−0.911 ± 0.009	0.992 ± 0.001
1.0	0.49	68.4 ± 0.2	100.6 ± 0.04	−0.896 ± 0.009	0.941 ± 0.001
1.5	0.74	72.7 ± 0.2	100.7 ± 0.05	−0.907 ± 0.010	0.977 ± 0.002
2.0	0.99	73.2 ± 0.2	102.2 ± 0.04	−0.906 ± 0.009	0.975 ± 0.001

[a] Abbreviations: k Boltzmann's constant, T temperature (absolute).

[b] Melittin concentration in the aqueous phase used to prepare the Winsor-III system and the aqueous subphase of BME for Winsor-IV systems.

[c] (Overall) melittin concentration in BMEs.

TABLE 4

Zones of inhibition (mm) for well diffusion of each treatment using the Polysorbate 80/ethanol Winsor-IV bicontinuous microemulsion (BME) system[a,b,c]

	Gram-negative bacteria		Gram-positive bacteria			
Treatment	***Escherichia coli* K12**	***Acinetobacter baumannii***	***Pseudomonas aeruginosa***	***Enterococcus faecium***	***Staphylococcus aureus***	***Streptococcus pyogenes***
Gentamicin[d]	30.67 ± 0.45^{A}	30.33 ± 0.96^{A}	30.50 ± 0.39^{A}	30.25 ± 0.89^{A}	28.67 ± 0.38^{A}	31.17 ± 0.79^{A}
0 g/L, BME[e]	12.67 ± 0.19^{C}	14.00 ± 0.24^{B}	13.50 ± 0.20^{C}	14.67 ± 0.30^{B}	13.83 ± 0.28^{C}	14.17 ± 0.28^{B}
1 g/L, BME[f]	14.00 ± 0.24^{B}	14.67 ± 0.30^{B}	14.33 ± 0.19^{BC}	15.50 ± 0.39^{B}	14.67 ± 0.30^{B}	15.33 ± 0.19^{B}
2 g/L BME[f]	13.50 ± 0.20^{B}	14.67 ± 0.38^{B}	14.67 ± 0.30^{B}	15.17 ± 0.15^{B}	14.50 ± 0.20^{BC}	14.83 ± 0.44^{B}
1 g/L, aqueous[g]	2.00 ± 0.00 ^{E}	2.50 ± 0.20^{D}	2.33 ± 0.38 ^{E}	2.17 ± 0.15^{D}	2.00 ± 0.00 ^{E}	1.50 ± 0.20^{D}
2 g/L, aqueous[g]	5.00 ± 0.00^{D}	4.00 ± 0.28^{C}	4.17 ± 0.15^{D}	4.17 ± 0.15^{C}	4.00 ± 0.00^{D}	4.83 ± 0.15^{C}

[a] Zones were corrected by subtracting the diameters of the well, 5 mm, from each measurement.

[b] Error bars represent standard error, calculated using a 95% confidence interval.

[c] Letter that are different represent statistically significant differences in mean values comparing BME treatments with and without melittin at a 95% confidence interval.

[d] Positive control.

[e] BME without melittin.

[f] BMEs encapsulated with melittin; co-listed are the melittin concentrations (1.0 or 2.0 g/L_{aq}) within the BME's aqueous subphase; overall melittin concentrations are given in Table 3.

[g] Aqueous solutions of melittin at given concentrations that mimic the aqueous solutions within the BME phases, including the presence of glycerol; serve as controls.